Report On Technical Tools For Post Disaster Damage Assessment

Submitted to:
The National Institute for Hometown Security

Submitted by:
The Pacific NorthWest Economic Region (PNWER) Foundation
Northeastern University

Prepared by:
Jerry F. Hajjar, Taskin Padir, Peter Boynton, Steve Flynn, Phil Anderson, Yujie Yan, Zhong Mao, Jiahao Wu, Unver Akmandor

26 September 2018

1. Introduction

1.1. Problem Statement

Both natural events and potential terrorist attacks will disrupt normal operations of lifeline infrastructure sectors. Consequently, rapid response and recovery capabilities would clearly benefit from leveraging a growing interest by major infrastructure owners and operators in using autonomous or human-supervised technological assets to support the inspection and maintenance of infrastructure assets. For example, railroad operator BNSF has been experimenting with the use of human-supervised small unmanned aerial systems (sUAS) to conduct remote examination of the condition of their rail tracks to support routine maintenance and repair. These same assets have the potential to be repurposed in the aftermath of a disaster to assess disaster sites so as to detect infrastructure damages and support data-driven decision making processes at emergency response centers. This project envisions that sUAS can serve as a ubiquitous tool for emergency management teams in the near future. However, for this to happen, industry, the public sector, and applied researchers must collaborate on the development of 1) human-supervised sUAS control, 2) human-sUAS interaction, 3) data analysis for damage detection capabilities, and 4) the concept of operations for using human-sUAS in a post disaster environment.

The primary aim of this project is to demonstrate the potential of leveraging sUAS in support of incident management processes during times of emergencies to save lives and to support the rapid recovery of critical infrastructure in the aftermath of catastrophic events. The project focuses on the metro-Seattle area while leveraging applied research on post-disaster infrastructure resilience in the metro-Boston area. This makes sense for three reasons: First, PNWER has ongoing relationships with key industry partners that have a major corporate presence in the Pacific Northwest, but have national reach; e.g., Boeing, Amazon, Microsoft, AT&T, and BNSF. Second, as a result of FEMA's "Cascadia Rising" national exercise in 2016, there is significant awareness of the vulnerability of critical infrastructure in the event of a major earthquake and a recognition that stepped-up efforts need to be made to improve planning for the post-mega-quake recovery of critical infrastructure. Third, the link with Greater Boston Area facilitates the connection to key Boston-based industry partners; e.g., MassRobotics and Unmanned Aerial Systems Development (UASD) as well as bi-coastal sharing of the result of this project, facilitating the national-level adoption of key findings and recommendation.

1.2. Project Goals

The project engages multi-state, multi-sector lifeline CI owners and operators to work with Northeastern experts in defining specific requirements on how drones could

increase the cost-effective resilience of infrastructure in the Pacific Northwest region. The project develops cost-effective tools that can be implemented by CI owners and operators to enhance their response and speedy recovery from any CI disruption. The project encourages major private sector partners (e.g., Amazon, BNSF, and Boeing) to develop protocols for deploying their sUAS during a major emergency to support post-disaster response and recovery in regions throughout the country. We organize our proposed work into two core objectives:

Objective 1: Rapid Infrastructure Modeling and Analysis. We use a low-flying sUAS to capture the geometry and appearance of a structure or site with high accuracy. The process consists of three key operations to be led by Co-PI Padir: 1) controlling the sUAS and creating a 3D point cloud map; 2) transforming the point cloud data into a semantic, component-based model; and 3) visually analyzing the model to identify defects. The product of this modeling process is a representation of the infrastructure that links together the robot's raw observations (e.g., 3D measurements, imagery, and pose data), the low level, point-cloud model, and the semantic, component-based model.

Objective 2: Damage Inspection and Assessment. Using the results of the model described in Objective 1, this work develops methods for documenting damage to highlight key areas of concern. This is done through a combination of heuristic techniques and machine learning based on a catalogue of damaged elements. The heuristics is based on core civil engineering expertise of Co-PI Hajjar, coupled with the expertise on emergency response from Co-PIs Holdeman, Boynton, and Flynn. These innovations are made possible by the unique combination of robotics, computer vision, civil engineering, and emergency management expertise that our multi-disciplinary team brings to the project. This project lays the scientific and technological foundations of UAS autonomous motion planning and damage detection for steel and concrete elements. The project enhances our understanding of the design requirements and operational principles for a new class of sUAS to support the ongoing monitoring and maintenance of our infrastructure. This work enables the realization and fast-deployment of open-hardware and open-software aerial manipulators that can be customized and assembled cost-effectively. The goal is to use rapid prototyping techniques that can support the means to remotely inspect our nation's critical infrastructure after natural disasters. The tight integration of the proposed thrusts in compositional autonomy and nondestructive anomaly detection and damage prediction hold the potential to transform how emergency managers respond and recover from natural disasters. A control and communication framework is designed to unify novel perception, planning and navigation, and human-robot interaction techniques. The sUAS, with different sensors selected

based on the mission scenarios, develops flight plans to confine itself to areas of interest for automated inspection. The “perception system” developed for the sUAS continuously inform the operator about the state of the environment and the assets. All systems is designed to be informed of their state and configuration and predict and avoid failures such as collisions or being stuck. Successful completion of this project will provide adaptable sUAS designs and sound data that establishes ranges and trade-offs of performance for a number of uses, leading to development of protocols for realistic deployment scenarios. While the focus of this work is on deployment of a single sUAS, future work can expand to have a fleet of sUAS deployed for coordinated use. In addition, while the focus of this work is on post-disaster assessments, much of this work will also be applicable to pre-event (including routine) inspections of infrastructure.

1.3. Project Outcomes

The project team will recruit and oversee a public-private critical infrastructure resilience task force to guide the project throughout its entire life-cycle. PNWER will be able to quickly assemble this team by leveraging two of its existing working groups in the region (1) the Transportation Recovery Working Group, and (2) the Supply Chain Resilience Working group. Participants in PNWER’s working groups include: Boeing, Microsoft, BNSF, AT&T, Puget Sound Energy, Amazon, NW Seaport Alliance, Port of Seattle, Port of Tacoma, Amtrak, BP, Washington Dept. of Transportation, King County Office of Emergency Management, King County Water and Waste Water, Seattle Dept. of Transportation, WA Military Dept., Tacoma Power, and Snohomish PUD. The task force will be engaged through a series of workshops and stakeholder engagement activities organized by PNWER to include stakeholder meetings that are already scheduled for related purposes throughout the performance period of this project. 2. The project team will undertake a regional inventory in the Pacific Northwest of public and private drone assets that are currently being used for non-emergency applications with the objective of identifying those that might be leveraged for use after a major disaster to support the assessment process. The project team will be enlisted to develop the design requirements for sUAS to best support damage assessments that can smoothly interface with current best practices in information gathering and management within the ICS framework. 3. The project team will develop a dataset for sUAS navigation and infrastructure damage detection. 4. The project team will vet the findings included in the technical report prepared at the end of the project. 5. The project team will solicit feedback from stakeholders in preparing a usability report for deploying sUAS to perform post-disaster infrastructure assessments. 6. The project team will organize and convene a table top exercise to engage multi-state and multi-sector CI owners and operators to examine how the

project outcomes can be applied to high risk scenarios in the Pacific Northwest region and beyond.

2. Experimental Procedures and Validation of Algorithms

2.1. Description of the Hardware Used in Validation

Two commercially available UAS platforms have been used within the scope of this project, (i) Erle-Hexacopter (Fig. 1a) and (ii) DJI M600 Pro (Fig 1b). Erle-Hexacopter uses a custom autopilot with a payload up up to 1kg. DJI M600 Pro designed for both indoor and outdoor operations and it can provide a flight time ranging from 18 min (maximum payload) to 38 min (no payload) with body weight of 9.5kg and total takeoff weight up to 15.5kg. For both platforms, the human-in-the-loop control is achieved by a radio-link controller. Erle-Hexacopter enabled pilot training and validation of preliminary development work early in the project timeline whereas the modified DJI M600 Pro has been the hardware platform used for validation of algorithms due to the flight time and payload capacity it provided. It also comes with an integrated communication module that allows a data transmission for distances up to 5 km.

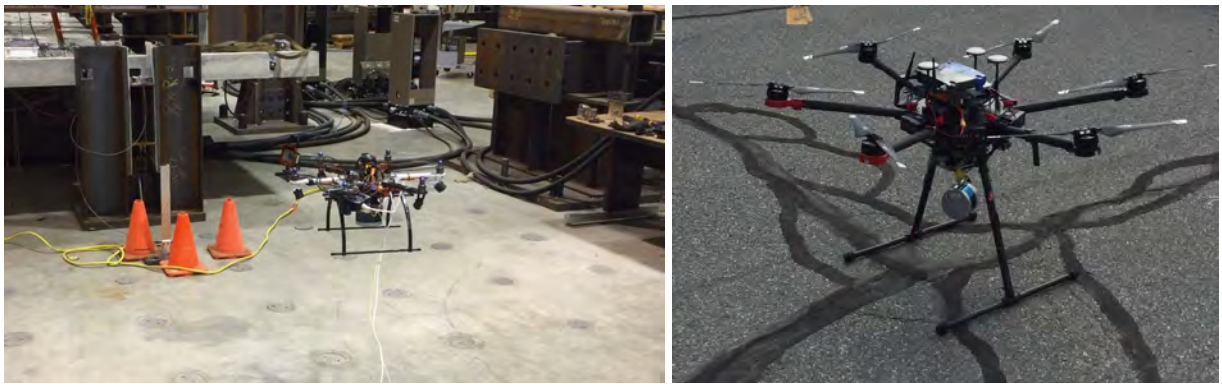

(a) (b)

Fig. 1. a) Erle-Hexacopter equipped with a fixed Lidar at the bottom; b) DJI M600 Pro equipped with a Lidar connected with a continuously rotating gimbal.

All algorithms developed within the scope of the project relies on raw data from a Lidar (light detection and ranging) sensor which collects three dimensional distance information utilizing the time-of-flight for a sweep of invisible light beams. In our modified UAS design, the Lidar sensor is chosen to be the Velodyne VLP-16, a 16 channel 3D Lidar with 0.1°-0.4° horizontal and 2° vertical resolutions. The Lidar sensor covers a view of 360° horizontally and 30° vertically. The maximum measurement range is 100 m with an accuracy of 3cm. Lidar sensor returns a point cloud as its output, which contains 3D position and intensity for each point. In order to improve the accuracy of the system the Lidar sensor is mounted on a single degree of freedom (DOF) gimbal under the DJI M600 Pro. The gimbal provides a continuous rotation of the sensor to expand

the Lidar sensor's 30° scanning view into 360° spatially. The design of the gimbal is shown in Fig. 2.

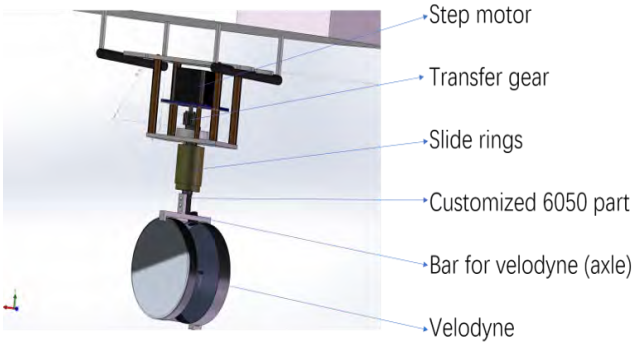

Fig. 2. The structure of the gimbal.

All on-board computation is performed on a high-performance embedded computer running Linux Ubuntu as the operating system and Robot Operating System (ROS) as the communications and data transfer framework within the software architecture. The variety of computer ports and payload capacity allows for integration of additional sensors and on-board data processing. A wifi communication network is established for the UAS using an on-board LINKSYS router.

2.2. Description of the Software Platform

We evaluated several Ground Control Station (GCS) software platforms for the project and selected the DJI's Ground Station as the GCS user interface. DJI Ground Station can be used for communications and for monitoring system parameters or variables during the mission scenarios. It can also be used for designing high-level trajectories by selecting way-points on a known map of the environment.

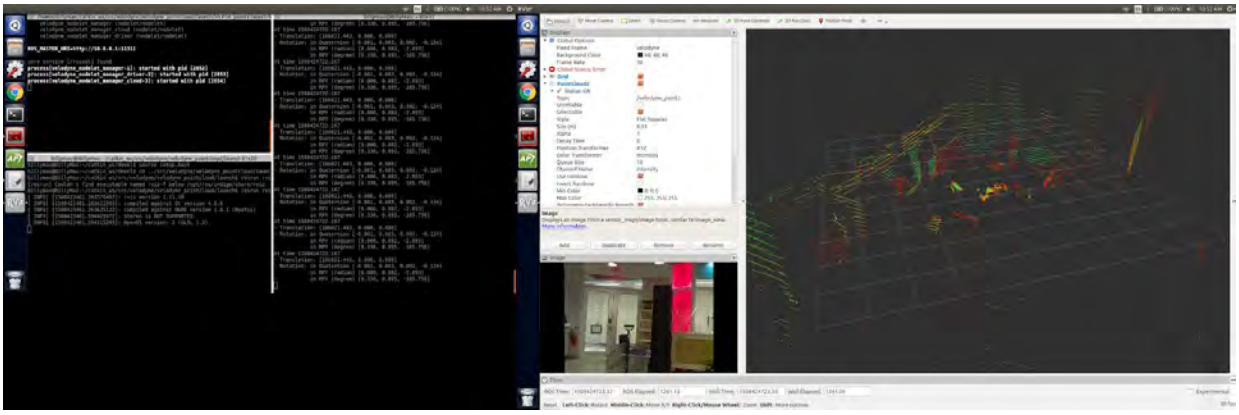

Fig. 3. ROS command interface and the real-time Lidar sensor point cloud visualization.

ROS is a flexible data distribution framework accelerating robotics research and development. It provide a collection of tools, libraries, and conventions that aim to simplify the task of creating complex and robust robot behaviors across a wide variety of robotic platforms. ROS also enables development of more advanced algorithms such as complicated trajectory design, and data processing. Fig. 3 depicts the ROS interface and the visualization tool it provides for the Lidar sensor point cloud data.

2.3. Validation of UAS Control Algorithms

Within the scope of the project, we developed both human-in-the-loop and semi-autonomous control algorithms for the UAS. The prerequisite for a successful flight to obtain accurate sensor data relies on stabilizing the position and attitude of the UAS. This is a challenging task especially especially when there is significant external disturbance present during the flight caused primarily by the weather conditions. Navigation in indoor environments suffer from the lack of GPS signal hence the localization needs to rely on the Inertial Measurement Unit (IMU) based estimation algorithms. GPS information can be used to evaluate the localization confidence together with IMU in outdoor missions. As we continue to develop our navigation algorithms, we relied on validation in simulation environments (Fig. 4). Under human operation, a remote controller is used to send flight command and receive messages from sUAS via wireless telecommunication. In autonomous flight mode, the sUAS is programmed to follow a predesigned trajectory, for example, a path that goes around the interesting location so that the scanning of complete external structure information can be covered.

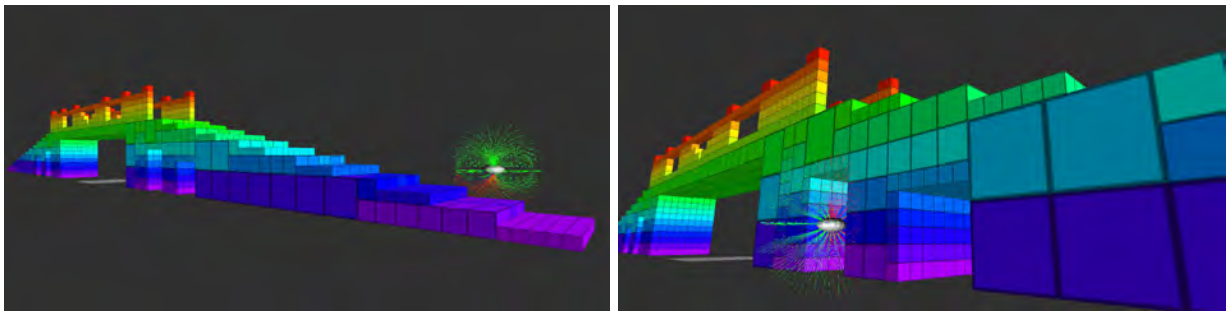

Fig. 4. Validation of autonomous path planning algorithms around a bridge in the simulation environment. Our work continues with the implementation of this algorithm on the actual platform.

Our human-in-the-loop flight control algorithms have been validated at the UAS Lab located at Northeastern University's Kostas Research Institute in Burlington, MA. The drone cage - which stands more than five stories tall and is 150 feet wide by 200 feet long - is large enough for two research groups to fly different drones simultaneously. The access to this lab has been an invaluable capability for our research and development team considering the overhead involved in securing necessary permits to perform outdoor testing. Fig. 5 provides an overview of the outdoor drone cage.

Fig. 5. UAS Lab drone cage located at Northeastern's Kostas Research Institute located in Burlington, MA.

2.4. Validation of Damage Detection Algorithms

Throughout the project timeline, numerous experiments have been performed in order to validate the developed damage detection algorithms. Experiments have been performed both indoors and outdoors with data collected from the lidar sensor with UAS being stationary and in flight. Furthermore, algorithms have been developed and validated for processing the data online during the flight as well as offline for processing after the completion of the mission.

Online Mapping. The validation of online mapping is part of the Simultaneous Localization and Mapping (SLAM) algorithm developed to achieve autonomous UAS flight. This capability allows the UAS to map its environment and localize itself within that map to explore unknown critical infrastructure. The map is updated using the point cloud data from the lidar sensor. We performed tests to validate our online mapping algorithm in numerous different scenarios.

1. **Online mapping in the lab environment:** The first experiment is conducted in the The Laboratory for Structural Testing of Resilient and Sustainable Systems (STReSS Laboratory) at Northeastern University. The experiment generated data collected from the Erle-Hexacopter equipped with a fixed Lidar sensor. The point cloud map representing the laboratory environment is depicted in Fig. 6.

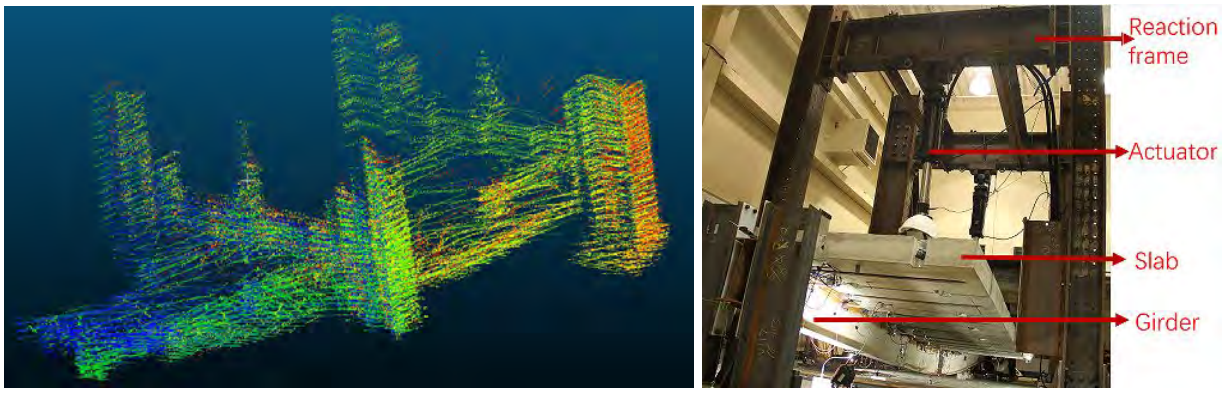

(a) (b)

Fig. 6. a) The 3D point cloud model of the structure in the STReSS Lab, and ceiling and floor are segmented away for visualization; b) the girder and slab are bent due to the loading of actuator.

2. **Improved online mapping in the lab environment:** In the second experiment, the Lidar sensor is mounted on the spinning gimbal and data is collected while the gimbal is kept stationary. The opening of an existing door in the Lidar sensor's view is used to simulate a gap with varying sizes. Fig. 7 depicts the representation of the door and its close vicinity segmented out of the whole map for visualization. The door gap size are kept at 15 cm and 5 cm respectively and the operator can visually recognize the door and the gap clearly (Fig. 7) and by the gap detection algorithm developed within the scope of this project (Fig. 8).

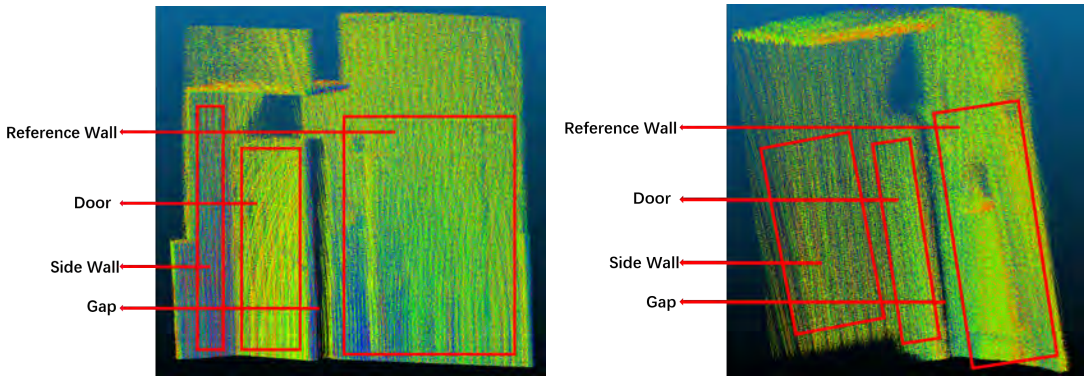

(a) (b)

Fig. 7. We use a door in our lab to simulate a gap model. The gap size is adjusted between 15 cm and 5 cm in (a) and (b) respectively.

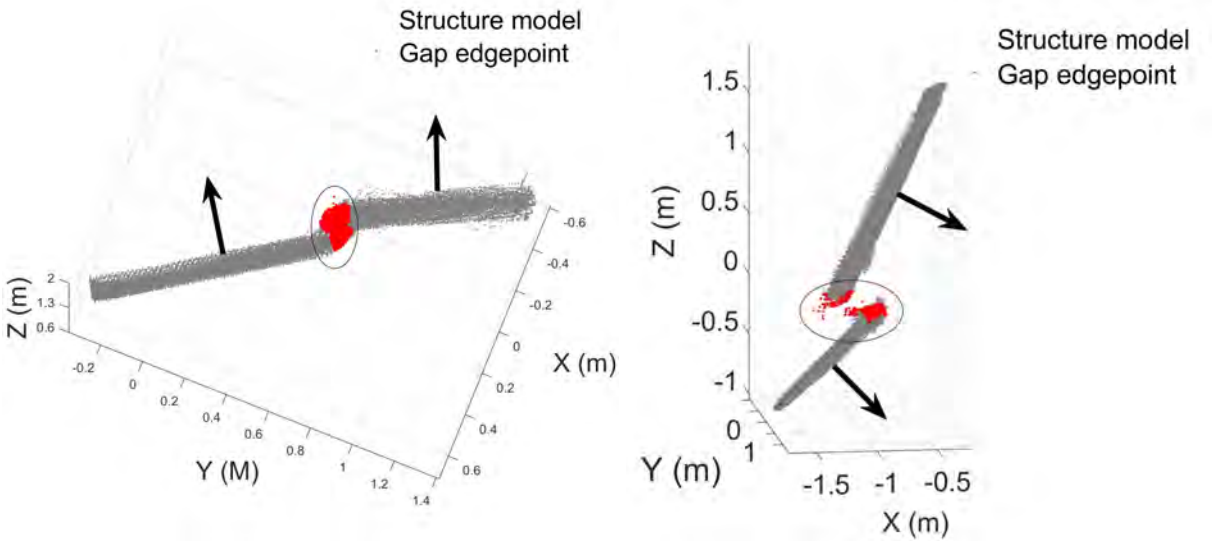

(a) (b)

Fig. 8. The 5 cm and 15 cm gaps are detected automatically in (a) and (b) respectively, where the red dots indicate the gap edge points and the arrows represent typical surface normal of wall and door plane.

3. **Improved online mapping in the lab environment:** In this validation experiment, the Lidar sensor is kept stationary in the STReSS Lab to obtain a holistic map of the environment. The ceiling and ground planes are segmented out to focus the analysis on the side walls and other structures forming the lab. As it can be seen from Fig. 9 that the entire lab is modeled uniformly and the reaction frame and the slabs can be recognized from the operator's view.

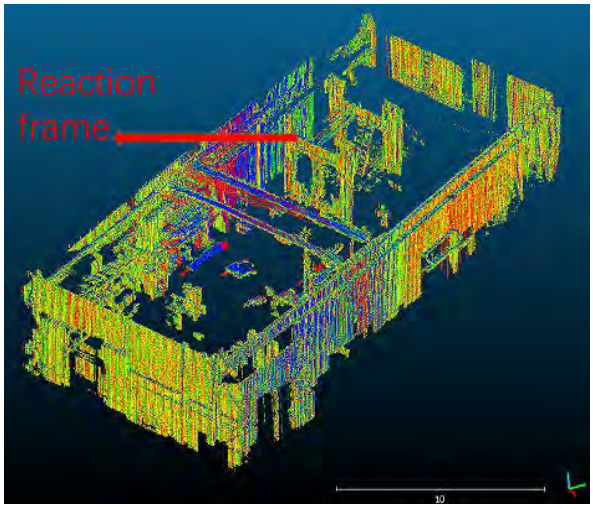

Fig. 9. The 3D map of the STReSS Lab obtained by the online mapping algorithms.

(a) (b)

Fig. 10. a) sUAS outdoor tests performed inside the netted enclosure supported by 14 poles; b) the online point cloud map of the netted enclosure.

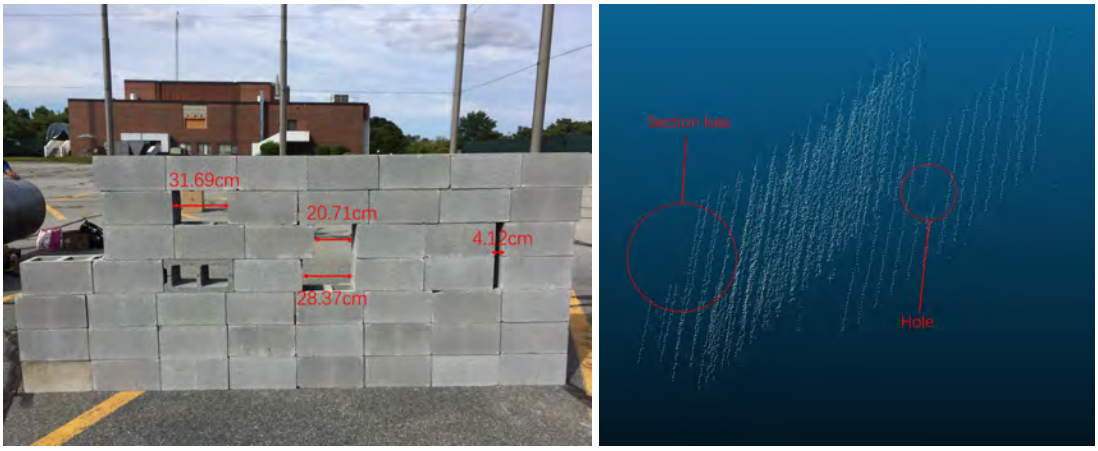

(a) (b)

Fig. 11. a) We build a wall that contains several "damages" using concrete blocks. There's a unfilled corner at left top and the size of gap and holes are labeled in red; b) the "double" wall is caused by mapping distortion in point cloud registration and the hole and missing corner are still recognizable.

4. **Improved online mapping outdoors:** In this validation experiment, the UAS carrying the Lidar sensor mounted on the gimbal is utilized inside the netted enclosure supported by 14 concrete poles (Fig 10a). The gimbal speed is set to 3 rpm. The online map generated by the system is shown in Fig. 10b and it contains 2 Lidar sensor sweeps. Even if there exist visible distortions in the map features, it matches the actual environment to provide operator with situational awareness about the environment. In order to improve the mapping process that relies on features in sensor data we add structures such as walls made from

concrete cinder blocks, which is shown in Fig. 11, using concrete blocks. In spite of the errors accumulating between each sensor sweep in Fig. 11, the hole and the missing corner representing damage are recognizable in the map from the operator view.

5. **Improved online mapping with repeatable damaged structures:** In this experiment, the UAS inspects the damaged structures outdoors but the gimbal is kept stationary to obtain comparative results. In order to simulate post-disaster damage, we build a continuous infrastructure (railway or pipeline) with section loss and bending to simulate to common types of damages (Fig. 12a). The Lidar scans the railway from top and the bend and the missing gap can be visually observed in the operator view.

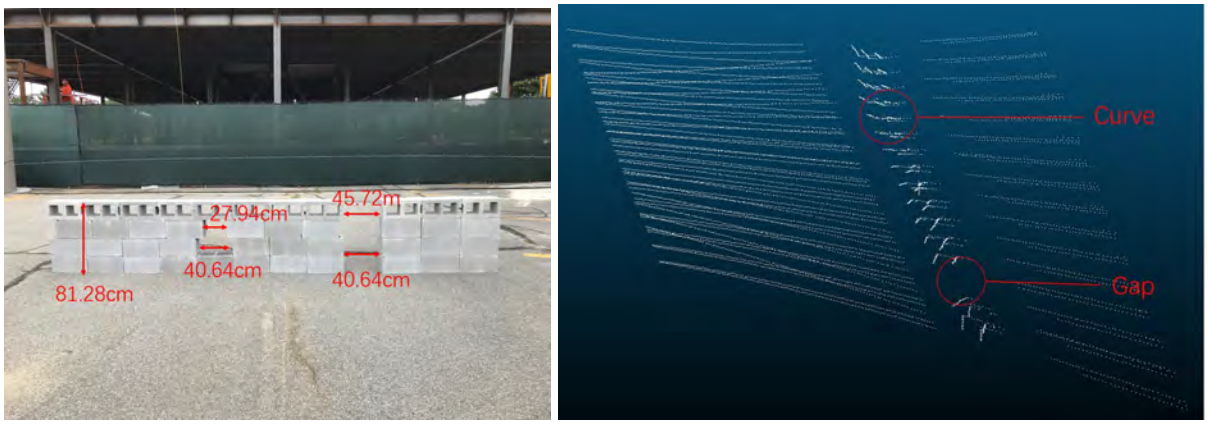

(a) (b)

Fig. 12. a) A continuous infrastructure that contains section loss and bend using concrete blocks, and the sizes are labeled; b) the missing gap and the railway bend are recognizable and the point cloud scans are taken while the Lidar sensor is above over the structure.

Offline Mapping. In order to improve the accuracy of our damage detection methods, we also developed offline map generation algorithms that require longer computation times running on our computer servers. The mission scenario here is to deploy the UAS as a data collection platform only and process the gathered data for processing in the mission control center later to perform the assessment.

1. **Offline mapping in the lab environment:** In the first step, the mapping algorithm is validated against dataset collected from the STReSS Lab. During this experiment, the Lidar sensor was placed stationary on ground with the gimbal rotating at a frequency of 2 RPM continuously in order to observe the environment with 360° field of view in the horizontal plane. The sensor is rotating internally as well at a speed of 600 RPM in order to obtain a 360° field of view in the vertical plane. This experiment is designed to validate the two key processes

of the mapping algorithm separately: formulation of local maps; and the registration between consecutive local maps. The local maps, as shown in Fig.13a is generated through integrating the points perceived from each scan, the rotation of the gimbal between scans and a pre-calibrated transformation matrix. The registration between local maps are then completed through a coarse registration based on Fast Point Feature Histogram (FPFH) and a fine registration using Iterative Closest Point (ICP) algorithm. The resultant point cloud map is shown in Fig. 13b.

The point cloud of the reaction frame and beam test specimen is segmented manually from the point cloud map for validating the semantic perception algorithm. This step is accomplished based upon the prior knowledge that the reaction consists of W-shape steel members and the beam test specimen consists of a W-shape steel beam and a concrete slab on top of it. Given the prior knowledge, the algorithm is capable of identifying the most of W-shape steel members and the concrete slab from the point cloud map as shown in Fig.14a. It is important to note the algorithm fails to detect two of the leaning steel beam in the reaction frame because no data was observed at the web of the steel beams.

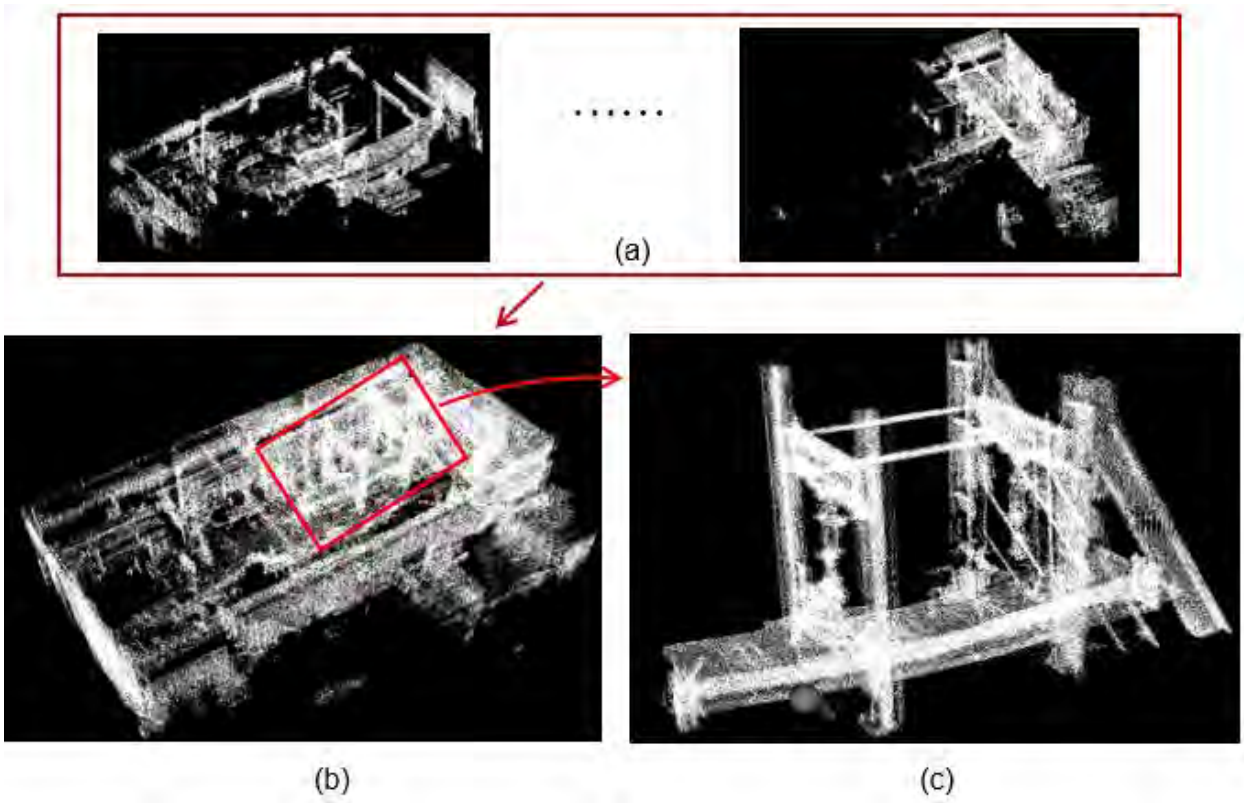

Fig. 13. STReSS Lab datasets: a) individual local maps; b) registration of local maps: c) point cloud of the beam test specimen

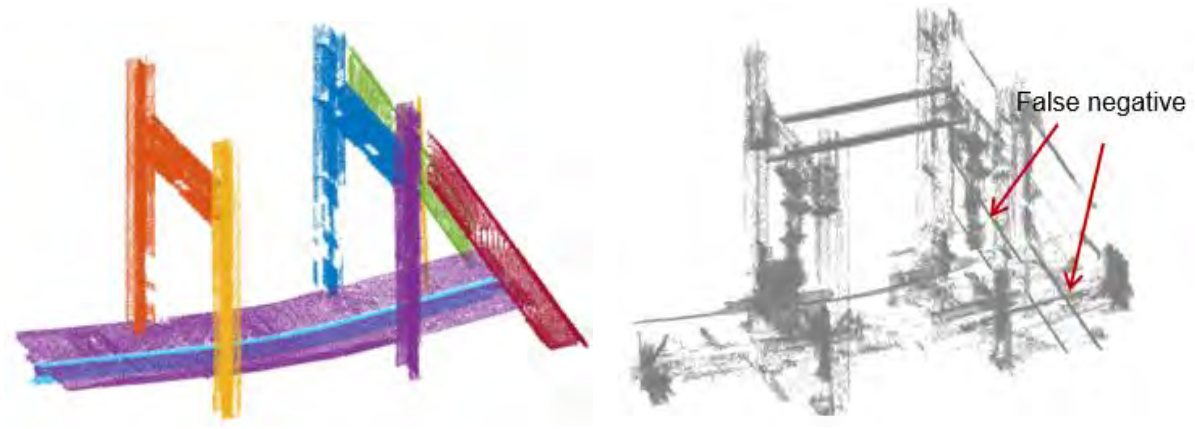

(a) (b)

Fig. 14. Beam test specimen: a) identified structural elements; b) remaining point after removing all structural elements

2. **Offline mapping using data from outdoor missions:** To illustrate the performance of the mapping algorithm against outdoor environment, we tested the algorithm against those datasets collected during the experiments in the sUAS facility located at Kostas Research Center. An example of the resultant point cloud maps is shown in Fig. 15a. For collecting this specific dataset, the sUAS platform flew fairly smoothly inside the sUAV facility under human piloting. IMU sensors is collecting the pose, angular velocity and acceleration of sUAS platform at a frequency of 400 Hz and the GPS is collecting the positional information at a frequency of 10 Hz. The Lidar sensor is rotating internally at 1200 RPM internally to acquire data in the vertically plane and is spinning at a 12 RPM through a gimbal to acquire data in the horizontal plane. The resultant point cloud map is shown in Fig.15a and the point clouds of a reference steel frame and experimental specimens are shown in Fig.13b and Fig.13c respectively. The accuracy of the point cloud mapping can be demonstrated through the wall contained in Fig. 13c. It is indicated that all synthetic damage in the walls (as shown in Fig. 11a) can be reflected in the point cloud map except the ‘crack’ with a thickness of 4.12 cm.

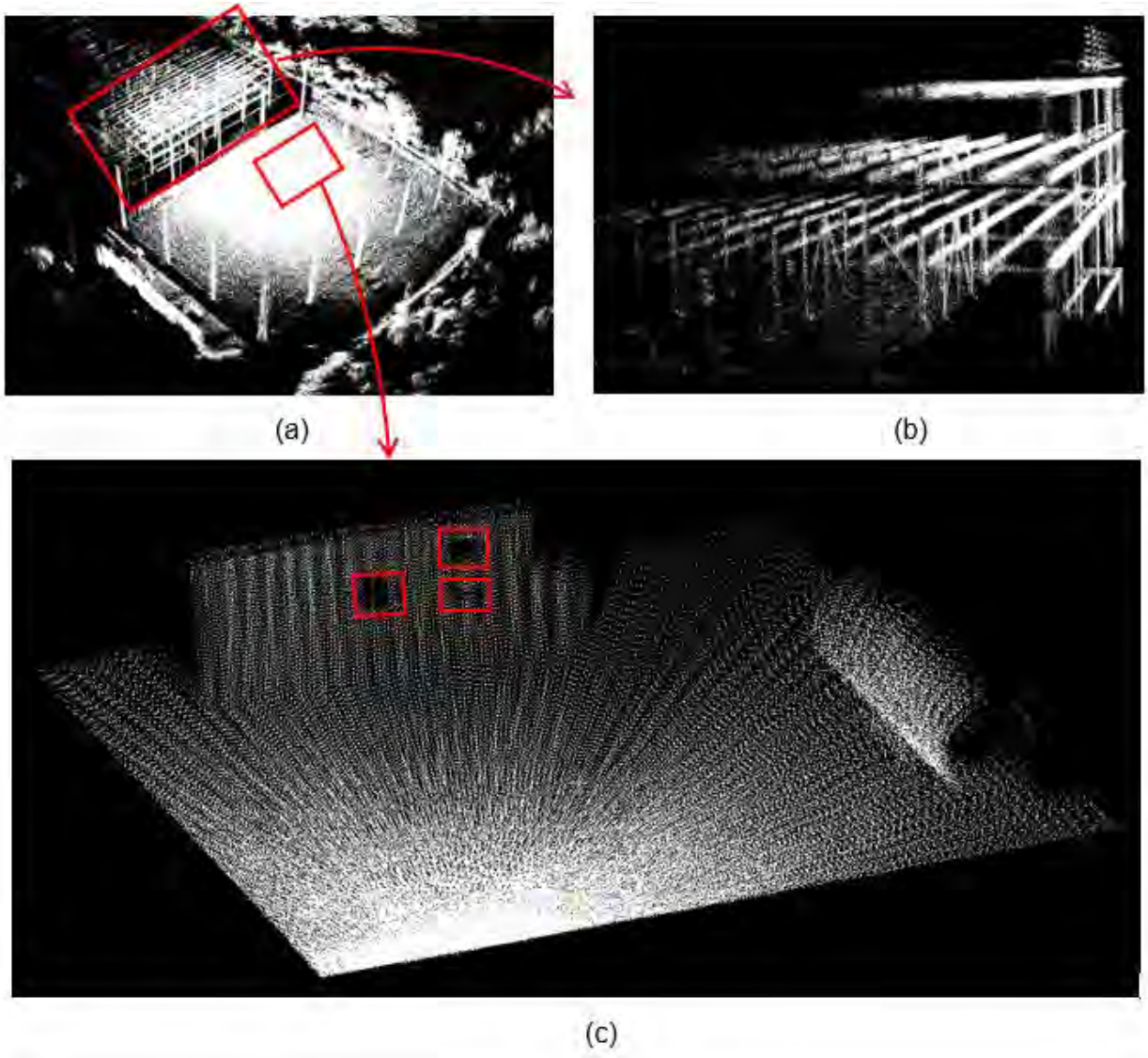

Fig.15. Selected sUAS Lab datasets: a) point cloud map; b) point cloud of the steel frame; (c) point cloud of the wall and steel tube inside the sUAS facility

The point cloud of the steel frame (as shown in Fig. 16b), which is located besides the the UAS Lab, is segmented manually from the point cloud map for validating the semantic perception algorithm. Since the sUAS platform is allowed to fly inside in the sUAS facility only, the point cloud of the steel frame is acquired at a distance of 20m – 65m from one point of view. This leads to a relatively incomplete and noise data, especially for members along X-axis. As such, it can be observed that most of the beams along Y-axis are identified successfully as shown in Fig. 16a, while the beams along X-axis are not.

(a) (b)

Fig.16. Steel frame: a) identified structural elements; b) remaining point after removing all structural elements

Validation of damage detection: The validation sets used for the damage detection algorithms are collected from several experimental specimens and one in-service bridge. The obtained results indicate that the damage detection algorithm is capable of localizing various types of structural damage effectively, as well as capturing their dimension with an acceptable accuracy. Several types of structural damage are investigated in this project including concrete spalling, steel section loss, localized buckling and bending of steel members, all of that will potentially to occur in structures and infrastructures after major disasters.

The performance of the proposed damage detection algorithm on detecting damage with small deformation is validated against datasets collected from a reinforced concrete pier cap of a railway bridge. A significant concrete spalling with reinforcement exposure can be observed at the corner of the pier cap. The key dimensions of the spalling are measured on point cloud dataset acquired by a terrestrial laser scanner and are shown in Fig. 17a. The same pier cap is then scanned using Velodyne VLP-16 equipped on a sUAS platform and the acquired point cloud data are processed using the surface normal-based damage detection algorithm. The results, as shown in Fig. 17b, indicate that the algorithm is capable of locating the concrete spalling effectively. The key dimension are also computed by the algorithm and are compared to those obtained from the terrestrial laser scanner data. It can be observed that the accuracy of capturing the width of the concrete spalling is high while that of the length is relative lower. The reason to this phenomenon is that the concrete spalling contains a crack-like tail on the left which is barely captured by laser point cloud due to the errors induced by laser measurement and mapping.

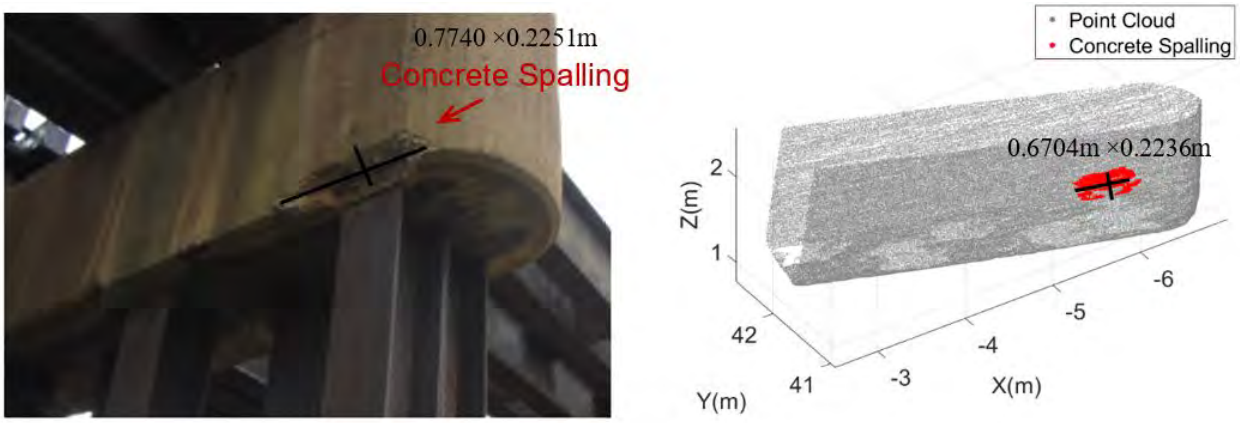

Fig.17. Detection of section loss and local buckling: a) image of the structure and damage; b) point cloud and damage detection results

The detections section loss and localized buckling are demonstrated through a circular tube specimen as shown in Fig 18a. The overall results are obtained using the graph-based method are shown in Fig. 18b. The point clouds are acquired by Velodyne VLP-16. It is observed that the algorithm locates and captures the contour of the section loss effectively. The key dimensions of the section loss are computed and compared with dimension obtained by micrometer. The results indicate that the overall error for capturing the dimension of the section loss is within ±10%. As the accuracy of laser measurements and mapping improves, we expect higher accuracy can be achieved. This example also indicates that the region of localized buckling, marked as red, can be identified effectively by the algorithm.

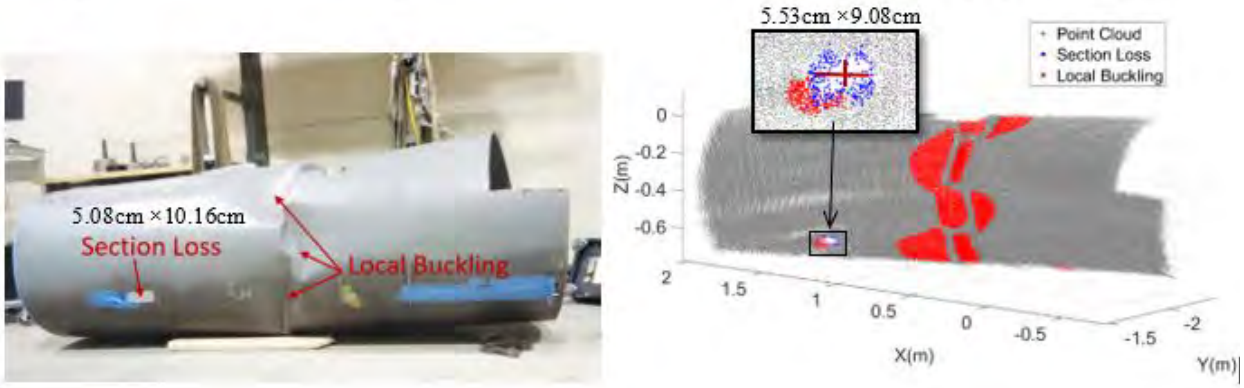

(a) (b)

Fig.18. Detection of section loss and local buckling: a) image of the specimen and damage; b) point cloud and damage detection results

The example of detecting bent members is explained using a wide flange steel beam that is subject to significant bending in the vertical direction after a beam test in

STReSS Lab (Fig.19a). A skeleton model need to be formulated in the first step in order to capture the deformation of the structural members. Once the skeleton model is extracted using the graph-based method (Fig.19b), the deformation is computed under the assumption that the member is initially straight. Such constraints can be released if the as-designed condition, in the form of either point cloud model or geometry model, is available. In order to evaluate the accuracy of proposed algorithm, the computed deformations are validated against the deformations measured using 5 displacement transducers that are placed at a distance of 1.829m, 3.048m, 4.877m, 6.706m, 7.925m to the end of the beam respectively. The results, as shown in Fig.17c, reveals that the algorithm computes the deformation of the steel beam with a maximum error of 6.4%.

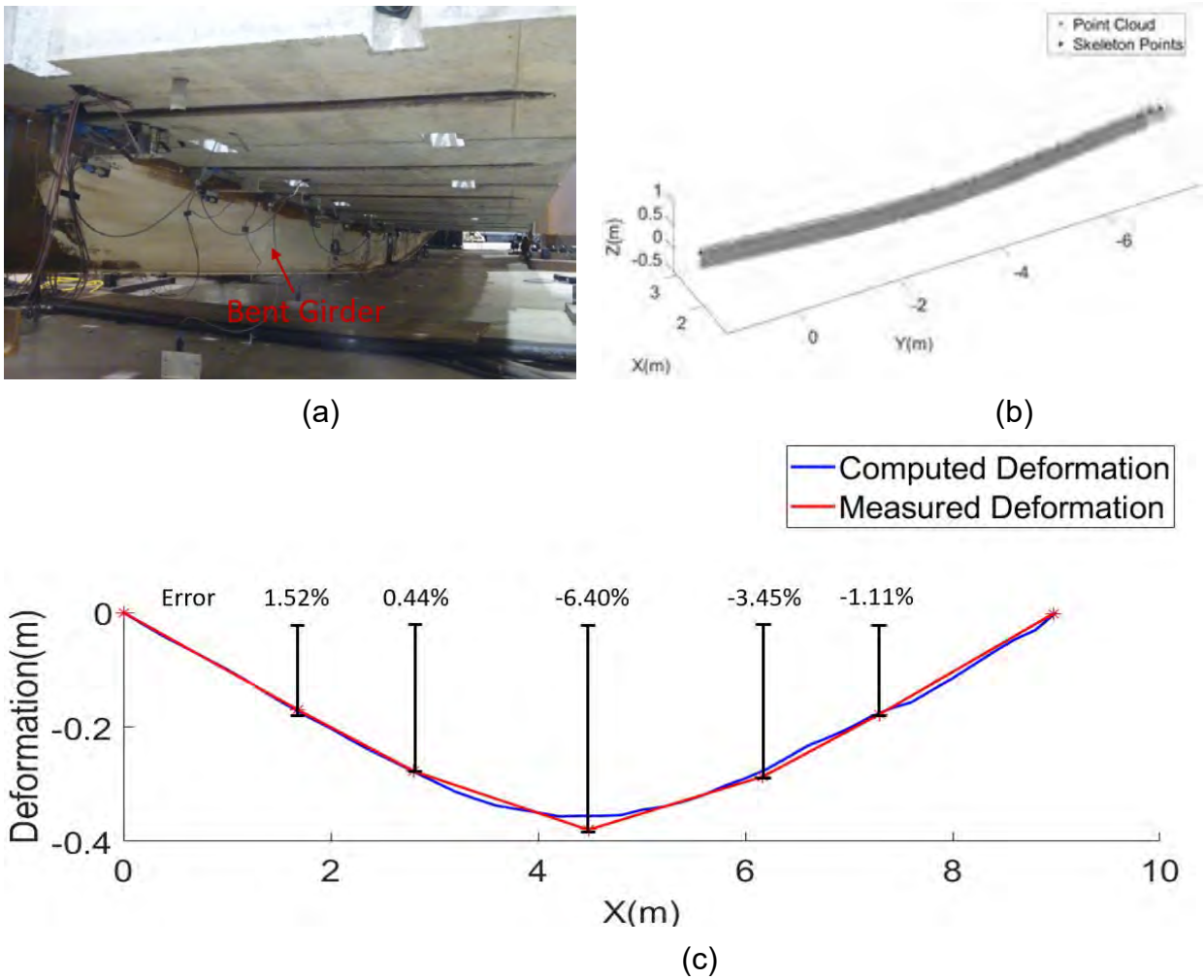

Fig. 19. Detection of section loss and local buckling: a) image of the specimen and damage; b) point cloud and damage detection results

3. Transition to Use and Accessibility of Tools

The research and development plan outlined in this project is aimed at taking a bold step towards achieving post-disaster damage assessment by nonconventional uses of UAS. As part of our transition to use strategy, we are maintaining a project website (http://www.coe.neu.edu/research/radar/index.html) and make our progress available to the community in the form of technical reports, videos and software repositories. As articulated in our motivation, inspectors, engineers and technicians who work on disaster recovery will benefit from this research and development effort. We will include an update on the accessibility of tools that are ready to share in our final report on algorithms.

4. Status and Ownership of Intellectual Property

This project has not yet produced any intellectual property.

5. Papers published acknowledging this award

1. Zhong Mao, Jiahao Wu, Yujie Yan, Jerome Hajjar, Taskin Padir, “Towards Automated Post-Disaster Damage Assessment of Critical Infrastructure with Small Unmanned Aircraft Systems”, 2018 IEEE International Symposium on Technologies for Homeland Security, Woburn, MA, Oct 23-24, 2018.